Hou *et al. Cell Communication and Signaling* (2025) 23:117
https://doi.org/10.1186/s12964-025-02108-z

Cell Communication and Signaling

RESEARCH Open Access

Lysine 2-hydroxyisobutyrylation of HXK1 alters energy metabolism and K_{ATP} channel function in the atrium from patients with atrial fibrillation

Hai-Tao Hou[1,2†], Xiang-Chong Wang[1,2,3†], Huan-Xin Chen[1,2], Jun Wang[1,2], Qin Yang[1,2] and Guo-Wei He[1,2,4*]

Abstract

Background Atrial fibrillation (AF) is the most common form of arrhythmia and is a growing clinical problem. Post-translational modifications (PTMs) constitute crucial epigenetic mechanisms but modification of lysine 2-hydroxyisobutyrylation (K_{hib}) in AF is still unknown. This study aimed to investigate the role and mechanism of K_{hib} in AF.

Methods PTM proteomics was applied in the human atrial tissue from AF and sinus rhythm patients with heart valve disease during cardiac surgery to identify the K_{hib} sites. The functional changes of differential modification sites were further validated at the cellular level. Cellular electrophysiology was performed to record the ion channel current and action potential duration (APD).

Results The modification of 124 K_{hib} sites in 35 proteins and 67 sites in 48 proteins exhibited significant increase or decrease in AF compared to sinus rhythm. Ten K_{hib} sites were included in energy metabolism-related signaling pathways (HXK1, TPIS, PGM1, and ODPX in glycolysis; MDHC and IDH3A in tricarboxylic acid cycle; NDUS2, ETFB, ADT3, and ATPB in oxidative respiratory chain). Importantly, decreased HXK1 $K418_{hib}$ regulated by HDAC2 attenuated the original chemical binding domain between HXK1 and glucose, inhibited the binding ability between HXK1 and glucose, and reduced catalytic ability of the enzyme, resulting in low production of glucose-6-phosphate and ATP. Further, it also increased Kir6.2 protein and the current of K_{ATP} channel, and decreased APD.

Conclusions This study demonstrates the importance of K_{hib} to catalysis of HXK1 and reveals molecular mechanisms of HXK1 $K418_{hib}$ in AF, providing new insight into strategies of AF.

Keywords Atrial fibrillation, Catalysis, 2-hydroxyisobutyrylation, Post-translational modification, Acylation

†Hai-Tao Hou and Xiang-Chong Wang are co-first author.

*Correspondence:
Guo-Wei He
gwhezj@163.com; gwhe@tju.edu.cn
[1]Institute of Cardiovascular Diseases, Department of Cardiovascular Surgery, TEDA International Cardiovascular Hospital, Tianjin University & Chinese Academy of Medical Sciences & Peking Union Medical College, No.61, 3rd Ave, TEDA, Tianjin 300457, China
[2]Tianjin Key Laboratory of Molecular Regulation of Cardiovascular Diseases and Translational Medicine, Tianjin, China
[3]Department of Pharmacology, Hebei Higher Education Institute Applied Technology Research Center on TCM Formula Preparation, Hebei International Cooperation Center for Ion channel Function and Innovative Traditional Chinese Medicine, Hebei University of Chinese Medicine, Shijiazhuang 050091, China
[4]Department of Surgery, OHSU, Portland, OR, USA

Introduction

Atrial fibrillation (AF) is the most common form of arrhythmia and is a growing clinical problem [1]. The prevalence of AF in the general population is as high as 2–3% and it is increasing annually [2] in patients with various etiological factors, including heart failure, hypertension, and valve heart disease [3]. Approximately 30% patients with AF suffer from some form of valve heart disease [3]. Studies revealed the mechanisms and pathophysiological alterations of AF, including atrial fibrosis [1], gene variant [4], histone deacetylases (HDACs) activation [5], ion channel dysfunction [6–8], glutathione metabolism [9], and microvascular dysfunction [10]. We have identified the role of peroxisome proliferator-activated receptor (PPAR) pathway in AF associated with valve heart disease [11]. However, the cellular and molecular mechanism of AF remains to be explored.

Post-translational modifications (PTMs) constitute crucial epigenetic mechanisms in regulating diverse biological events. Different short-chain and long-chain lysine acylations have been identified over the past decade [12–16]. These lysine acylations are not only associated with cellular functions, such as gene transcription and metabolism, but also physiology and diseases [17–19]. Lysine 2-hydroxyisobutyrylation (K_{hib}) is a novel acylation that regulates glycolysis [20]. Emerging studies revealed the roles of hib in common wheat [21], saccharomyces cerevisiae [22], and ustilaginoidea virens [23]. Although succinylation modification has been reported in AF [24], there is little research on the role of K_{hib} in human diseases.

In our preliminary experiments, four types of acylation (acetylation, succinylation, crotonylation, and K_{hib}) were screened in right atrial tissues taken from patients with AF or sinus rhythm (SR) who underwent heart valve surgery. K_{hib} was significantly different in AF and SR.

The present study was designed to reveal the role of K_{hib} in the development of AF associated with heart valve disease and particular attention was paid to identify pathways linked with metabolism.

Table 1 Patient characteristics of the proteomics/validation cohorts

Variables	SR ($n=13$)	AF ($n=13$)	*P*
Age	59.7 ± 1.9	56.2 ± 2.1	0.22
BMI	24.2 ± 0.7	24.4 ± 0.6	0.88
Smoking (%)	1(7.7)	4(30.8)	0.32
Alcohol (%)	0(0)	1(7.7)	1.00
Hypertension (%)	3(30)	1(7.7)	0.59
Hyperlipidemia (%)	1(7.7)	2(11)	1.00
Diabetes (%)	0(0)	1(7.7)	1.00
LVDD (mm)	48.2 ± 2.4	50.1 ± 1.8	0.55
LAD (mm)	48.1 ± 0.8	52.5 ± 1.4	0.01
LVEF (%)	60.3 ± 2.3	56.1 ± 1.7	0.15

SR, sinus rhythm; AF, atrial fibrillation; BMI, body massive index; LVDD, left ventricular diastolic disorder; LAD, left atrial diameter; LVEF, left ventricular ejection fraction

Methods

Human subjects

All the patients had mitral valve replacement and left atrial appendage closure due to rheumatic heart disease with mitral stenosis and mitral regurgitation.

During heart valve surgery, discarded right atrial appendages during the cannulation procedure were collected from AF and SR patients and immediately transferred to liquid nitrogen for preservation. The protocol was approved by the Ethics Committee of the TEDA International Cardiovascular Hospital (2019-0315-1). Informed consent was obtained before surgery. All samples were collected according to the principles outlined in the Declaration of Helsinki.

A total of 26 patients (13 for SR and 13 for AF) were enrolled in this study. The patients who had frequent ventricular premature beats or paroxysmal supraventricular tachycardia were excluded from this study. The patients were allocated into two groups as follows.

SR: $n=5$ (2 male and 3 female) for K_{hib} proteomics and $n=8$ (2 male and 6 female) for validation.

AF: $n=5$ (2 male and 3 female) for K_{hib} proteomics and $n=8$ (2 male and 6 female) for validation."

The demographic and clinical characteristics of the patients are presented in Table 1. Left atrial diameter [25] in AF group was significantly higher than that in SR. The LAD difference was also verified using logistic regression analysis (Table S1). The increase of LAD in the AF patients in this study is consistent with other clinical studies [26, 27].

Cell line culture

HL-1 atrial myocyte cell line was obtained from ATCC. HL-1 atrial myocytes are derived from atrial tumor (AT-1) cells of transgenic mice expressing the SV40 large T antigen under the control of the atrial natriuretic factor promoter, and can proliferate indefinitely [28] in Dulbecco's modified Eagle's medium supplemented with 10% fetal bovine serum at 37 ℃ with 5% CO_2.

Protein isolation and trypsin digestion

Total protein was extracted and digested into peptides with trypsin in two steps. The protein solution was reduced with 5 mM dithiothreitol for 30 min at 56 °C and alkylated with 11 mM iodoacetamide for 15 min at room temperature. The protein sample was then diluted by adding 100 mM tetraethyl ammonium bromide. Finally, trypsin was added at the ratio of trypsin to protein of 1:50 in the first digestion overnight, and at the second digestion for 4 h, the mass ratio of trypsin to protein of 1:100 was added.

Tandem mass Tag (TMT) labeling

Tryptic peptide was desalted by Strata-X C18 SPE column (Phenomenex), dried in vacuum, and labeled by TMT following the manufacturer's protocol. The peptide mixtures were then incubated for 2 h at room temperature and pooled, desalted, and dried by vacuum centrifugation. To enrich K_{hib} related peptides, TMT-labeled peptides were incubated with pre-washed antibody beads (PTM801, Jingjie PTM Biolab Co. Ltd, Hangzhou, China) at 4 °C overnight with gentle shaking and eluted with 0.1% trifluoroacetic acid.

LC-MS/MS

The peptide passed through a nanospray ionization source, and then it was subjected to MS/MS in Q ExactiveTM Plus (Thermo), which was connected with Ultra Performance Liquid Chromatography. The electrospray voltage applied was 2.0 kV. The scanning range of the full scan was 350 to 1800, and the intact peptides were detected in the Orbitrap with the resolution of 70,000. Peptides were then selected for MS/MS using normalized collision energy setting as 28 and the fragments were detected in the Orbitrap at a resolution of 17,500. Fixed first mass was set as 100 m/z. The data were processed using Maxquant search engine (v.1.5.2.8) to identify and quantify the K_{hib} related proteins. False Discovery Rate was adjusted to < 1% and minimum score for modified peptides was set > 40. The experiments were performed in Jingjie PTM Biolab Co. Ltd, Hangzhou, China.

Bioinformatics analysis

Three major GO categories (biological process, cellular compartment, and molecular function), domain annotation, protein-protein interactions, and KEGG enrichment of proteins with differentially expressed K_{hib} sites were analyzed. Enrichment-based hierarchical cluster based on differentially modified proteins was applied for functional classification.

Motif analysis

Modification motifs software (motif-x algorithm) was used to analyze the sequence model composed of amino acids at specific positions (10 amino acids upstream and downstream of this position). Protein sequences of all the database were used as background parameters. Minimum number of occurrences was set to 20. Emulate original motif-x was ticked, and other parameters were the same as the default values.

Western blot assay

Tissues or cells were lysed with the RIPA Lysis buffer (Beyotime) containing cocktail inhibitors (Thermo Scientific) at 4 °C. After centrifugation at 12,000 g at 4 °C for 10 min, the supernatant was collected and the protein concentration was determined by bicinchoninic acid kit (Beyotime, China) according to the manufacturer's instructions. Equal amount of protein in each sample was loaded to the sodium dodecyl sulphate-polyacrylamide gel electrophoresis. The proteins were transferred onto polyvinylidene fluoride membrane (Beyotime) and blocked with tris-buffered saline and tween 20 containing 5% non-fat dry milk for 1 h at room temperature, followed by incubation with the primary antibody overnight at 4 °C. The membrane was washed with tris-buffered saline and tween 20, incubated with horse radish peroxidase-conjugated secondary antibodies for 1 h at room temperature, and observed by ECL enhanced chemiluminescence detection system. Equal amounts of total protein were normalized by glyceraldehyde-3-phosphate dehydrogenase (GAPDH) as loading control.

Co-immunoprecipitation (Co-IP)

IP was conducted according to the manufacturer's instructions (Cell Signaling Technology, USA). In brief, tissues or cells were lysed on ice by IP lysis/wash buffer (pH 7.4, 25mM Tris, 150mM NaCl, 1mM EDTA, 1% NP40, 5% glycerol) containing protease and deacetylase inhibitor cocktail (Thermo Scientific & Beyotime) for 10 min. Protein was incubated with antibody-cross-linked A/G magnetic beads overnight at 4 °C. After being washed with elution buffer, the bound antigen was denatured and subjected to sodium dodecyl sulphate-polyacrylamide gel electrophoresis and immunoblotted with the indicated antibodies.

Histone deacetylase 2 (HDAC2) regulates K_{hib} of hexokinase-1 (HXK1)

Co-IP was applied to verify the interactive relationship between HDAC2 and HXK1. K_{hib} level of HXK1 was detected after adding a HDAC2 inhibitor (Trichostatin A, # 9950, Cell Signaling). Briefly, cells were cultured for 24 h and then treated for another 16 h with trichostatin A (400 nM). Cells were homogenized with lysis buffer and the supernatant was collected for K_{hib} detection.

Simulation of binding of substrate and enzymes

Auto-Dock 4.0 was used to dock small molecules (substrates) into their enzyme structures with or without K_{hib} modification, respectively. The original enzyme structure (HXK1) was obtained from the protein data bank database (https://www.pdbus.org/). The enzymatic structure with K_{hib} was generated by modifying the side chain of lysine using ChimeraX software. The structure of small molecule (glucose) was downloaded from Chemspider (http://www.chemspider.com/). In this study, the binding of HXK1 and glucose was simulated. The information on active sites and substrate binding sites of HXK1 were predicted by COACH. Before the docking simulation,

glucose was placed into the substrate binding site of enzyme as the start point of docking. The conformation with the lowest binding energy of glucose was considered as the enzyme-bound conformation. By comparing the binding energy and conformation of the enzymes with or without K_{hib} modification, we infer the effect of the modification on the enzymatic activity.

Assay of HXK1 activity

HL-1 cells were transfected in a 6-well plate using Lipofectamine 2000 (11668019, ThermoFisher Scientific) with pcDNA3.1 (vector), pcDNA3.1-HK1, and pcDNA3.1-HK1-K418R respectively. Cells were washed with PBS before imaging with an Olympus DP73 fluorescence microscope to evaluate the transfection efficiency. Cells were cultured for 48 and 72 h and then homogenized (1×10^6-10^7) with ice-cold lysis buffer and centrifuged at 10,000 × g for 10 min. The supernatant was collected and used for the activity of HXK1 (Abcam ab136957, UK) following the manufacturer's instructions. The concentration was corrected by dividing by total protein.

Glucose-6-phosphate assay

The glucose-6-phosphate level was measured by assay kit (Sigma-Aldrich) according to the manufacturer's protocol. Briefly, cells were homogenized with cold PBS and centrifuged at 13,000 × g for 10 min. The supernatant was deproteinized with a 10 kDa molecular weight cut-off (MWCO) spin filter (UFC5010, Millipore). Fluorescence at 450 nm was measured ($n = 5$) using microplate reader (16039400, TECAN, Austria). All samples were run in duplicate. The concentration was corrected by dividing by total protein (ng/μL).

Adenosine 5′-triphosphate (ATP) assay

The ATP level was detected by enhanced ATP assay kit (Beyotime, China) according to the manufacturer's instructions. In brief, cells were washed thoroughly in cold PBS and lysed immediately with 200 μL buffer per well of 6-well plate. After centrifugation (12,000 × g) at 4 ℃ for 5 min, the supernatant was collected. Luminescence was detected using luminometer (Fluoroskan FL, ThermoFisher Scientific) to assess ATP content. Samples were analyzed with 2 technical replicates and 5 experimental replications ($n = 5$). The concentration was corrected by dividing by total protein (nmol/mg).

Electrophysiological measurements

The HL-1 atrial myocytes retain a highly differentiated cardiac morphological, biochemical and electrophysiological phenotype reflective of atrial cardiomyocytes [29]. The electrophysiologic features of HL-1 cells are similar to those of mammalian cardiac myocytes, and they have a variety of typical ionic currents [30]. In addition, the essential features of atrial tachycardia remodeling seen in animal models [31, 32] and human AF [33] were also preserved for HL-1 cells, which makes it a good experimental system for studying ion channel function and arrhythmia. The methods used in the present work for AP studies of HL-1 atrial myocytes have been well documented [29, 34].

Patch pipettes were fabricated from glass capillaries (OD, 1.5 mm; ID, 0.86 mm; length, 10 cm) using a Sutter P-1000 microelectrode puller (Sutter Instrument, USA). The whole-cell patch-clamp technique (HEKA, Germany) was used to record K_{ATP} current in the voltage-clamp mode. Cells were superfused with bath solution composed of (mmol/L): NaCl, 120; KCl, 20; $MgCl_2$, 1; $CaCl_2$, 2; glucose, 10; and HEPES 10 (PH = 7.4). Pipette microelectrodes were pulled using a programmable horizontal puller and had tip resistances of 2–3 MΩ, when filled with solution containing (mmol/L): K-aspartate, 100; NaCl, 8; KCl, 40; Mg ATP, 0.1; EGTA, 5; $CaCl_2$, 2; GTP Tris, 0.1; and HEPES 10 (PH = 7.2). The recording stimulation procedure was as follows: cells were clamped at -40 mV and stimulated with a step of 300 ms from − 80 mV to + 80 mV, with a step increase of 10 MV. The K_{ATP} channel inhibited by glibenclamide (10 μM) and HMR1098 (10 μM), and the K_{ATP} current was defined as glibenclamide and HMR1098 sensitive current. The current was normalized by cell capacitance into current densities (pA/pF).

The patch-clamp technique was also used to record the action potential (AP) in the current-clamp mode. Pipette solution contained (mmol/L) NaCl, 5; KCl, 20; potassium glutamate, 120; $MgCl_2$, 1; $CaCl_2$, 1; and HEPES, 10; MgATP, 2.5 (PH = 7.2). The external solution contained (mmol/L) NaCl, 138; KCl, 4; $MgCl_2$, 1; $CaCl_2$, 2; NaH_2PO4, 0.33; glucose, 10; and HEPES, 10 (pH 7.4). APs were evoked with a supra-threshold (1000 pA) current pulse of 5 ms duration at a rate of 1 Hz. The parameters of APs, including action potential duration at 30% repolarization (APD_{30}), APD_{50}, APD_{90}, action potential amplitude (APA) and resting membrane potential (RMP) were then analyzed in each group. The current and APD protocols were similar to previous studies [35, 36].

Statistical analysis

Data are presented as means ± SEM. P values were calculated using two-tailed unpaired Student's t-test when two independent groups were compared. When the ratio of AF/SR was more than 1.2 or less than 0.83, it was identified as significant up- or down-regulation. It is worth noting that all the K_{hib} -proteomics data reported in this study have been normalized by the general proteomics results of the same samples. Data were analyzed using SPSS 20.0 software (SPSS Inc., Chicago, IL, USA) and GraphPad Prism (version 7, GraphPad Software Inc.,

San Diego, CA). Comparisons that were statistically significant were labeled with * ($p < 0.05$), ** ($p < 0.01$), or *** ($p < 0.001$).

Results

Related proteins and sites analysis

Figure 1A shows the schematic overview of the experimental approach. Western blot assay showed the whole K_{hib} level between AF and SR (Fig. 1B). The expression of P300 (histone acetyltransferase) in AF was lower than that in SR (Fig. 1C). In contrast, HDAC2 in AF was higher than that in SR (Fig. 1D). A total of 6,523 matched spectrum, 3,234 peptides, 2,867 modified peptides, corresponding to 579 proteins and 2,900 sites from Liquid chromatography-tandem mass spectrometry (LC-MS/MS) analysis were identified (Fig. 1E). Of these identified proteins and sites, 480 proteins and 2,275 sites are quantifiable. The distribution of mass errors was near zero and most errors were less than 5 ppm, demonstrating that the mass data were qualified (Fig. 1F). Figure 1G and H show the number of K_{hib} sites per protein and peptide length distribution respectively. The length of most peptides distributed between 7 and 22, which is consistent with the length of tryptic peptides, indicating that sample preparation achieved a reasonable standard.

Differentially expressed K_{hib} sites analysis

Figure 2A shows that there were 124 K_{hib} sites related to 35 proteins exhibited upregulation in AF compared to SR. In contrast, 67 sites related to 48 proteins exhibited downregulation. Subcellular location analysis of these proteins revealed that cytoplasm, nucleus, and extracellular accounted for the most proportion (Fig. 2B). Figure 2C shows the feature sequence of the motif sites. The specific form can directly show the appearance of each amino acid. Figure 2D shows the motif enrichment heatmap of all the amino acids in the 10 upstream and 10 downstream locations. Each square represents a location, the middle column represents the K_{hib} sites. Figure 2E shows the specific mass spectrogram of HXK1 $K418_{hib}$ for its identification and quantification. Gene Ontology (GO) including biological process, cellular component, and molecular function, Kyoto Encyclopedia of Genes and Genomes (KEGG), and functional annotation analysis demonstrated that the K_{hib} related proteins were significantly enriched in the above analyses (Figure S1 and S2).

The results of mass spectrometry of HXK1 $K418_{hib}$ were also verified by Co-IP (Fig. 2F). Figure 2G shows the expression of P300, HXK1, and HDAC2 in HL-1 cells. Co-IP also verified the interaction between HDAC2 and HXK1 (Fig. 2H and I). Co-expression of trichostatin A (HDAC2 inhibitor) upregulated the level of HXK1 hib (Fig. 2J and K).

K_{hib} on key enzymes involved in glycolysis, Tricarboxylic acid cycle (TCA), and oxidative respiratory chain

In this study, ten differentially expressed K_{hib} sites (Fig. 3A and B) were found to be involved in glycolysis (HXK1, TPIS, PGM1, and ODPX), TCA circle (MDHC and IDH3A), and oxidative respiratory chain (NDUS2, ETFB, ADT3, and ATPB). Particularly, functional classification demonstrated that specific proteins were involved in 3 functions related to energy metabolism including carbohydrate transport and metabolism, energy production and conversion, and amino acid transport and metabolism (Fig. 3C and D).

Molecular docking was also used to simulate the binding conformation of HXK1 and its substrate (glucose) with or without $K418_{hib}$. In the presence of side chain modification (simulating high level of $K418_{hib}$, Fig. 3E), glucose formed a hydrogen bond with the modified K418. In addition, glucose also interacted with other three amino acids (Ser88, Arg91, Ser415) and formed total 9 hydrogen bonds. The binding energy is -7.07 kcal/mol. However, in the absence of side chain modification (simulating low level of $K418_{hib}$, Fig. 3F), glucose formed 12 hydrogen bonds with six amino acids (Thr172, Lys173, Asn208, Glu294, Glu260, Asp209), which led to an obvious binding site shift. The binding energy is -3.74 kcal/mol. Therefore, low level of $K418_{hib}$ attenuated the original binding domain between HXK1 and glucose (Fig. 3E and F), reduced the binding stability (from 7.07 to 3.74), and inhibited the binding ability between HXK1 and glucose. These changes eventually reduced the HXK1 activity.

K_{hib} reduced the enzyme activity and affected the energy production

Figure 4A and B show the experimental design and the reaction process of HXK1 and glucose. High transfection efficiency was observed by florescence assay (Fig. 4C). In addition, HXK1 protein levels significantly increased in the overexpressed compared with wild or empty vector pcDNA3.1 by immunoblotting (Fig. 4D, $p < 0.001$). Overexpression of HK1-K418R significantly reduced enzyme activity at 48 (Fig. 4E, $p < 0.001$) and 72 h (Fig. 4F, $p < 0.001$) compared to the overexpression of the normal HXK1.

HK1-K418R reduced the production of glucose-6-phosphate (Fig. 4G, $p < 0.001$) and downstream ATP (Fig. 4H, $p < 0.001$) compared with HXK1 normal overexpression.

HXK1 $K418_{hib}$ increased the current of K_{ATP} channel ($I_{K,ATP}$), reduced action potentials (APs), and increased the expression of Kir6.2

Patch clamp recording showed that the whole-cell K^+ current of HL-1 atrial myocytes was significantly inhibited

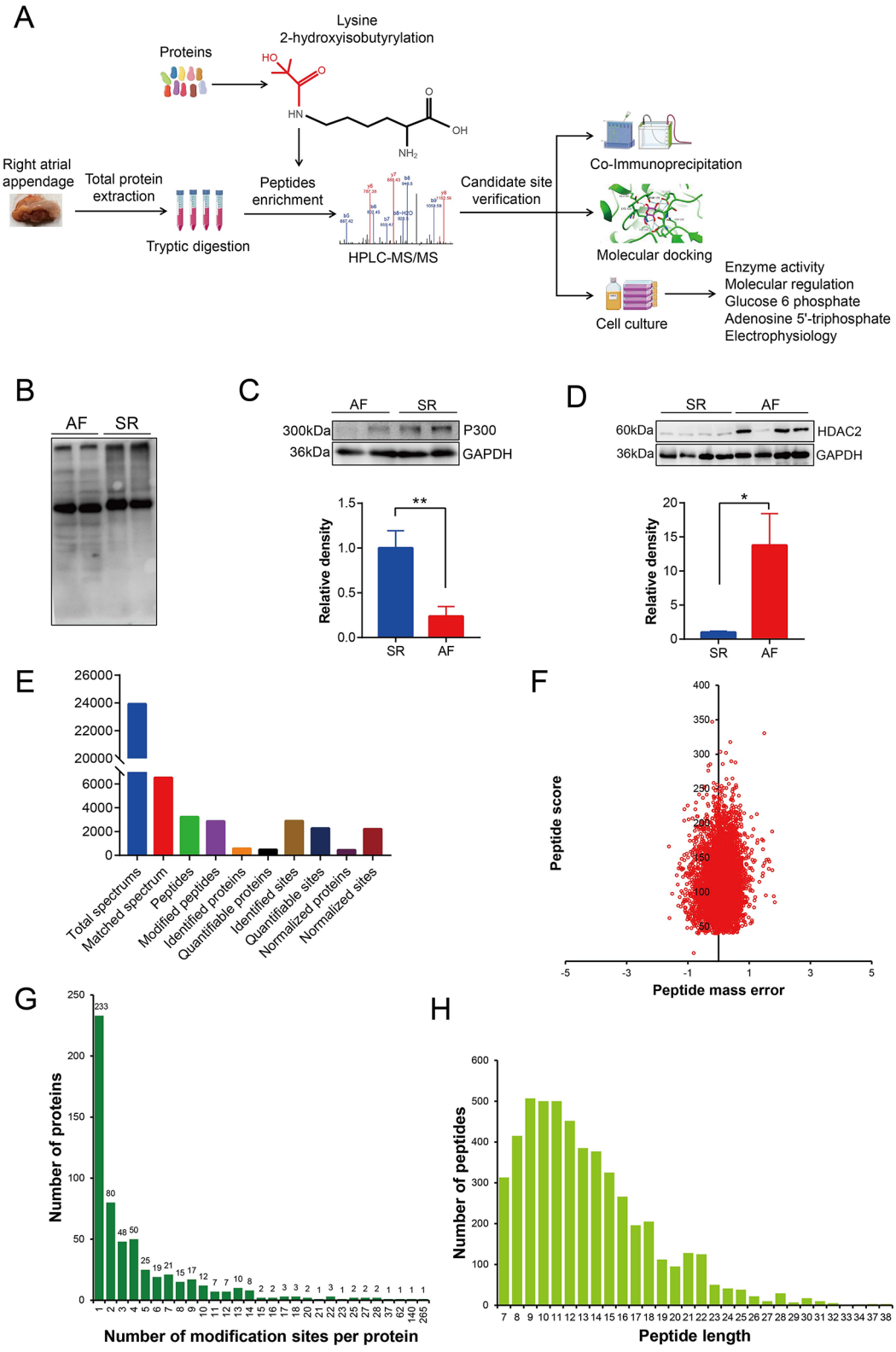

Fig. 1 Model workflow for identifying 2-hydroxyisobutyrylated proteins between human AF and SR. (**A**) The schematic overview of the experimental approach. (**B**) The whole lysine 2-hydroxyisobutyrylation level between AF and SR. (**C** and **D**) Expression of P300 ($n=5$) in AF was lower than that in SR. HDAC2 ($n=4$) in AF was higher than that in SR. (**E**) Spectrums, peptides, proteins, and sites identified by mass spectrometry. (**F**) Peptide mass error. Mass error indicates the accuracy of identified peptides. All the mass errors were smaller than 3 ppm, demonstrating good accuracy of the MS data. (**G**) Relationship between 2-hydroxyisobutyrylation sites and proteins. (**H**) Peptide length distribution. Most of the identified peptides were from 7 to 22, consistent with the length of tryptic peptides. AF, atrial fibrillation; SR, sinus rhythm. *$p<0.05$; **$p<0.01$ by unpaired t test. Data are presented as mean ± SEM

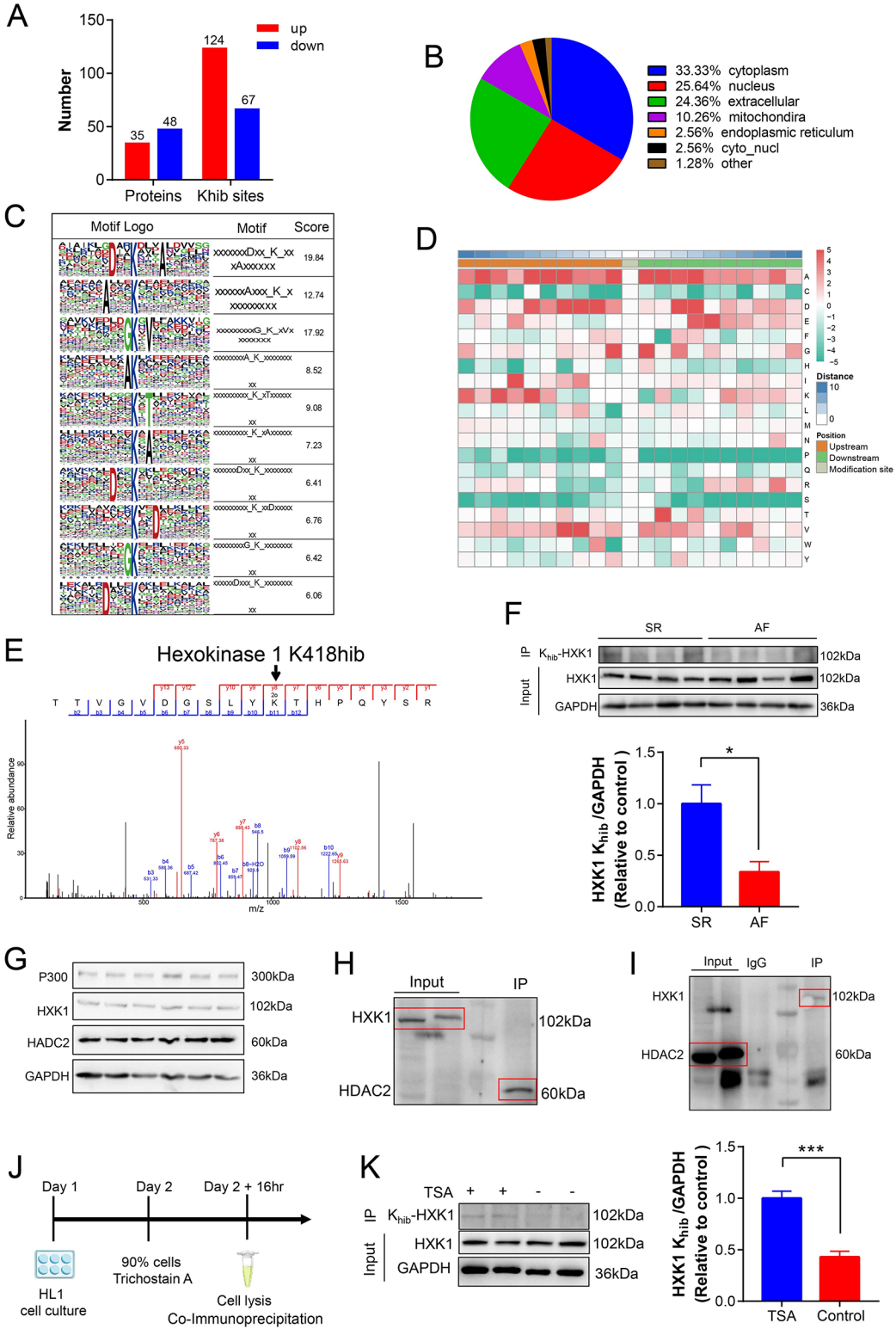

Fig. 2 (See legend on next page.)

(See figure on previous page.)

Fig. 2 The quantified differential 2-hydroxyisobutyrylated sites, typical motif, and regulation role of HDAC2 on HXK1. (**A**) Differentially expressed 2-hydroxyisobutyrylation sites and related proteins. (**B**) Subcellular distribution of above proteins. (**C**) Ten typical feature sequences of differentially expressed 2-hydroxyisobutyrylated sites. (**D**) The motif enrichment heatmap of upstream and downstream amino acids of all identified modification sites. Red color indicates that the amino acid is significantly enriched near the modification site, and green color indicates that the amino acid is significantly reduced near the modification site. (**E**) HXK1 peptides sequenced by mass spectrometry. b and y represent the fragment ions of the N and C termini in peptide backbone, respectively. m/z, mass-to-charge ratio. (**F**) HXK1 K_{hib} verification ($n=4$) by co-immunoprecipitation in human atrium. Tissue lysates were immunoprecipitated with anti-HXK1 antibody, followed by immunoblotting with a pan-2-hydroxyisobutyrylation antibody. (**G**) Expression of P300, HXK1, and HDAC2 in HL-1 cells ($n=6$). (**H** and **I**) Verification of interaction of HDAC2 and HXK1 by co-immunoprecipitation in HL-1 cells. (**J**) Experimental scheme. Trichostatin A, a HDAC2 inhibitor, was added when the HL-1 cell grew to 90%. Cells were lysed when trichostatin A was added for 16 h. (**K**) The level of HXK1 K_{hib} ($n=4$) increased after adding trichostatin A. AF, atrial fibrillation; SR, sinus rhythm; GAPDH, glyceraldehyde-3-phosphate dehydrogenase; HDAC2, histone deacetylase 2; HXK1, hexokinase-1; TSA, Trichostatin A. *$p<0.05$; ***$p<0.001$ by unpaired t test. Data are presented as mean ± SEM

by glibenclamide in HK1 (22.26 ± 1.26 vs. 15.59 ± 1.14 pA/pF, $p<0.001$) (Fig. 5A) and HK1 K418R (32.84 ± 1.95 vs. 19.98 ± 1.34 pA/pF, $p<0.001$) (Fig. 5B) groups. Figure 5C and D showed that HK1 K418R significantly increased the whole-cell K^+ current from 22.26 ± 1.26 pA/pF to 32.84 ± 1.95 pA/pF, which was proved to be largely due to the enhancement of K_{ATP} channel current. K_{ATP} channel blocker glibenclamide was used to distinguish $I_{K,\ ATP}$. After HK1 K418R treated, the difference of the $I_{K,\ ATP}$ currents induced by glibenclamide increased from 6.67 ± 0.37 to 12.89 ± 1.19 pA/pF ($p<0.001$) (Fig. 5E and F). Exposure of HL-1 atrial myocytes to HK1 K418R resulted in shortening of APD (Fig. 5G and H). Compared to HK1 group, APD_{50} decreased from 27.11 ± 2.09 to 18.26 ± 1.93 ms ($p<0.05$) (Fig. 5J) and APD_{90} decreased from 114.64 ± 8.67 to 73.21 ± 6.91 ms ($p<0.01$) (Fig. 5K), respectively. However, HK1 K418R did not affect APD_{30} (Fig. 5I), APA (Fig. 5L), and RMP (Fig. 5M).

Further, in order to verify the effect of HK1 K418R on the nature of these currents, HMR1098 (specific K_{ATP} channel inhibitor) was performed in the patch clamp study. HMR1098 significantly decreased the whole-cell K^+ current both in HK1 and HK1 K418R groups (Fig. 6A and B). HK1 K418R increased whole-cell K^+ current from 20.82 ± 1.32 to 35.42 ± 1.46 pA/pF ($p<0.001$) (Fig. 6C and D) significantly which attributed to the increase of the difference of the $I_{K,\ ATP}$ currents induced by HMR1098 (6.62 ± 0.79 vs. 14.95 ± 0.62 pA/pF, $p<0.001$) (Fig. 6E and F). The results suggested that HMR1098 have a similar effect as glibenclamide on K_{ATP} channel current.

Kir6.2 is the pore-forming component of the ATP-sensitive potassium (K_{ATP}) channel [37]. HK1-K418R expression significantly increased the expression of Kir6.2 (Fig. 5N, $n=6$, $p<0.05$) compared with HXK1 normal overexpression in HL-1 cell. Similarly, the expression of Kir6.2 in human atrial tissue with AF is also significantly higher than that in SR atrial tissue (Fig. 5O, $n=8$, $p<0.05$).

Discussion

The present study for the first time revealed larger number of differentially expressed K_{hib} sites between AF and SR in patients with valve disease. The proteins related to these sites are involved in diverse cellular processes, particularly the energy metabolism. Importantly, this study suggested that (1) glycolysis was inhibited by HXK1 $K418_{hib}$ site, resulting low level production of energy and (2) K_{ATP} current and APD were affected by HXK1 $K418_{hib}$ site that most likely triggers AF. Therefore, the present study for the first time emphasizes that HXK1 $K418_{hib}$ plays a critical role in regulating glycolysis metabolism, ATP production, and the current and APD of energy-related ion channels - K_{ATP}. These results provide insights into the AF mechanism related to metabolism and indicate that K_{hib} is involved in the metabolism of the atrium (Fig. 7). Further, HXK1 $K418_{hib}$ is an important acylation site in AF.

Regulation of HXK1 $K418_{hib}$

P300/CBP and HDAC2/HDAC3 have been reported as acyl-transferase (writers) and deacetylases (erasers) of hib respectively [38]. In this study, we found that the expression of P300 in SR was higher than that in AF (Fig. 1C) and HDAC2 in SR was lower than that in AF (Fig. 1D). HDAC inhibition has also been proved as a therapeutic intervention to maintain a healthy proteostasis in AF [39–42]. However, the specific molecular mechanism of HDACs inhibition in AF therapy remains unknown. In this study, we have verified the low expression of HDAC3 in the right atrium and we focused the study on the regulation of HXK1 K418hib by HDAC2. At last, we found that HDAC2 inhibition had role of upregulating HXK1 K_{hib} level and therefore this mechanism may become a therapeutic strategy of AF.

HXK1 $K418_{hib}$ reduced energy generation

Emerging evidence suggests that metabolic impairment and adenosine monophosphate-regulated protein kinase play crucial roles in the pathogenesis of AF [43, 44]. Excitation-contraction coupling in cardiac myocytes requires high amounts of ATP [45]. A study reported that HXK1-mitochondria association modulates pyruvate flux and ATP synthesis [25]. Nevertheless, there were no studies reporting the relationship among AF, HXK1, and ATP. In this study, we found that $K418_{hib}$ of HXK1 reduced

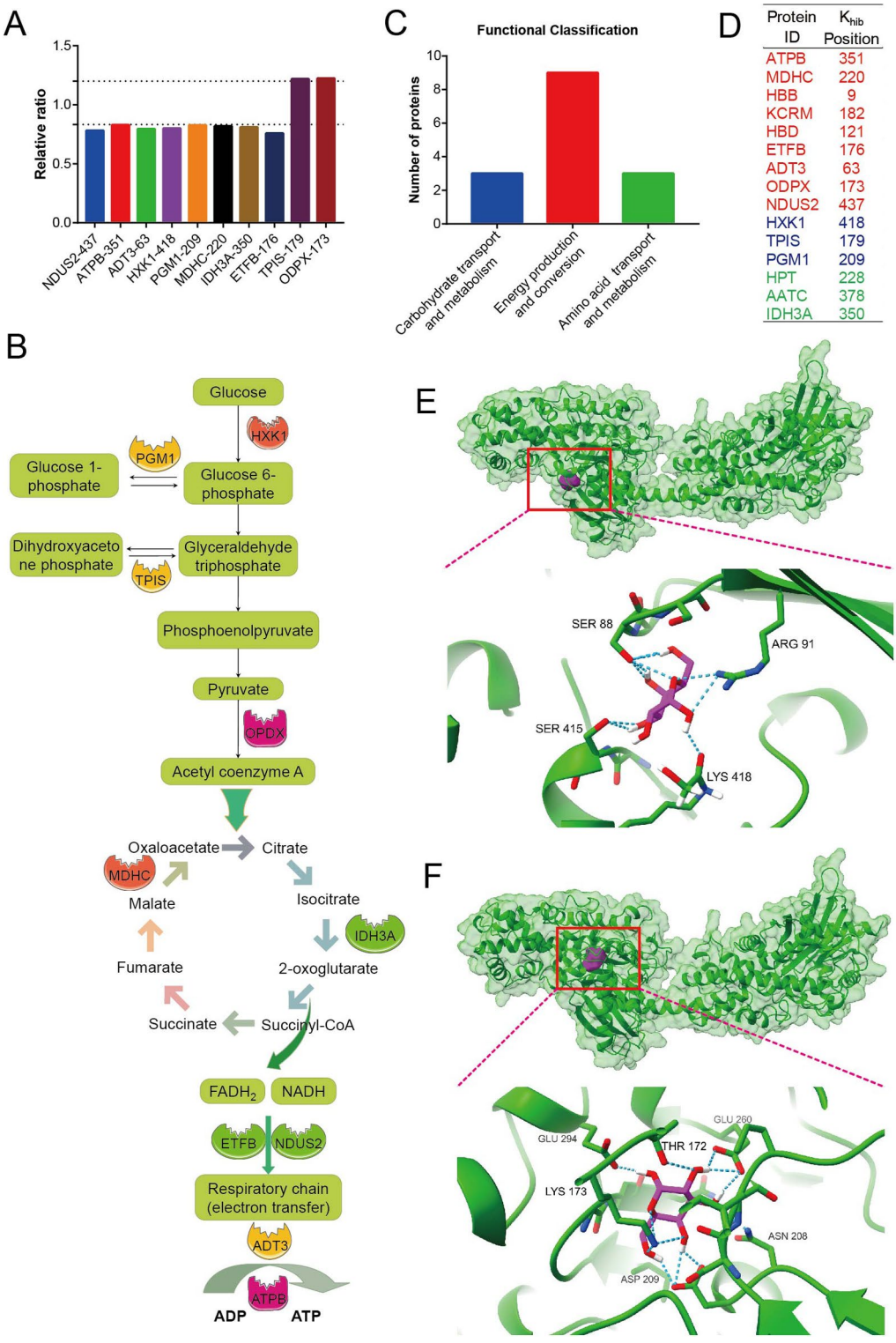

Fig. 3 Lysine 2-hydroxyisobutyrylated enzymes involved in energy production. (**A**) Summarized bar graphs depicting 10 key glycolytic enzymes that were identified as differentially expressed 2-hydroxyisobutyrylated sites. (**B**) Above 10 enzymes were involved in glycolysis (HXK1, TPIS, PGM1, and ODPX), TCA circle (MDHC and IDH3A), and oxidative respiratory chain (NDUS2, ETFB, ADT3, and ATPB). (**C**) Three functional energy classification of proteins corresponding to differentially expressed K_{hib} sites. (**D**) Specific proteins involved in above 3 energy functions. (**E**) In the presence of side chain modification (simulating high level of $K418_{hib}$). Glucose formed a hydrogen bond with the modified Lys418. Glucose also interacted with other three amino acids (Ser88, Arg91, Ser415) and formed total 9 hydrogen bonds. The binding energy is -7.07 kcal/mol. (**F**) In the absence of side chain modification (simulating low level of $K418_{hib}$). Glucose formed 12 hydrogen bonds with six amino acids (Thr172, Lys173, Asn208, Glu294, Glu260, Asp209). The binding energy is -3.74 kcal/mol

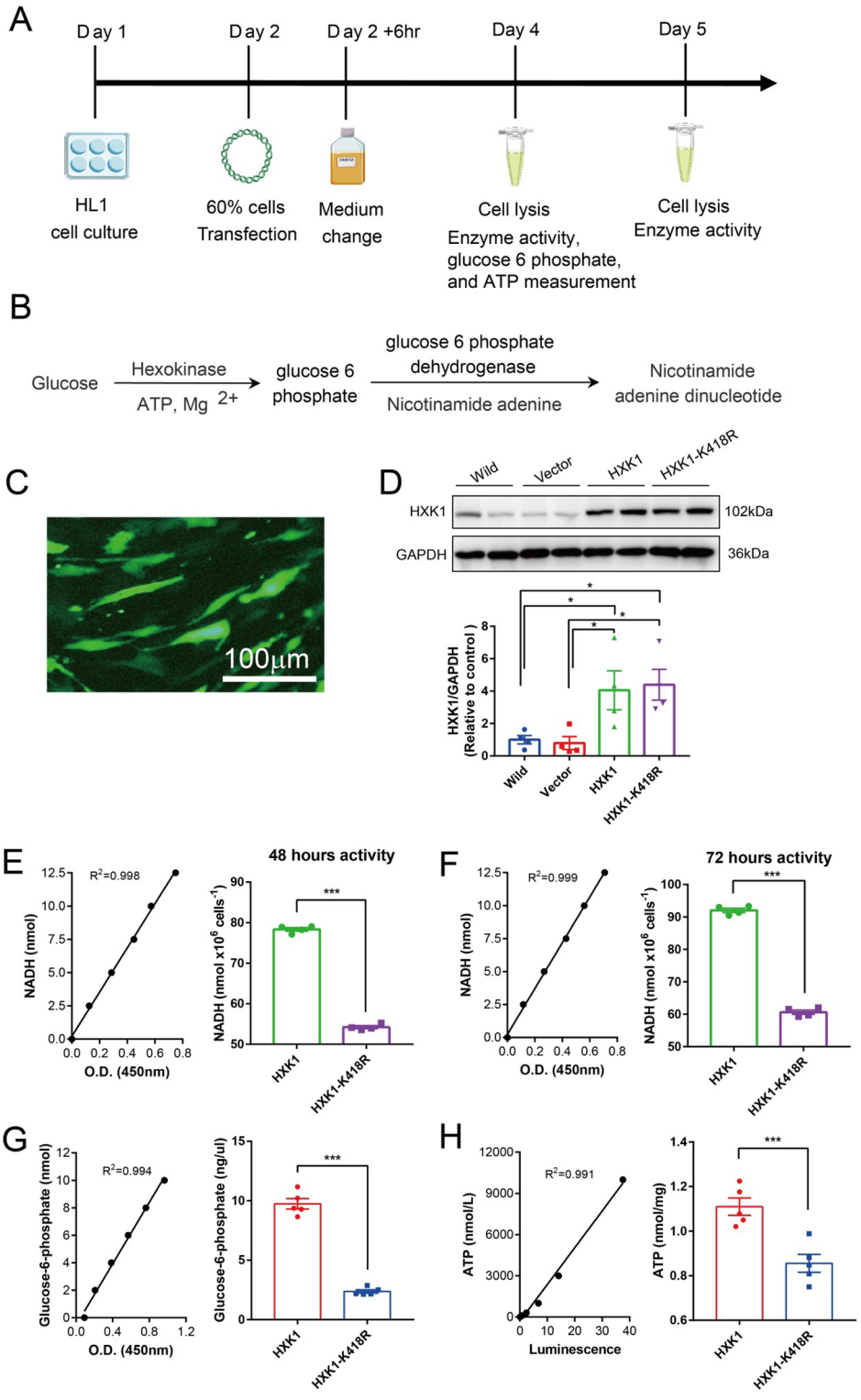

Fig. 4 Lysine 2-hydroxyisobutyrylation reduced HXK1 activity and energy production. (**A**) Experimental design. (**B**) Reaction process of HXK1 and glucoses. (**C**) Representative fluorescence assay exhibiting a high transfection efficiency in HL-1 cells. Scale bar, 100 μm. (**D**) Expression of HXK1 ($n=4$) in wild, empty vector PCDNA3.1, a vector encoding pcDNA3.1-HK1 (HXK1), and a vector encoding pcDNA3.1-HK1-K418R in HL-1 cells. (**E** and **F**) K418R group significantly reduced HXK1 activity at 48 ($n=4$) and 72 h ($n=4$) compared with HXK1 normal overexpression group. (**G** and **H**) HK1-K418R reduced the production of glucose-6-phosphate ($n=5$) and adenosine 5′-triphosphate (ATP) ($n=5$). HXK1, hexokinase 1; GAPDH, glyceraldehyde-3-phosphate dehydrogenase; NADH, nicotinamide adenine dinucleotide. $^{*}p<0.05$; $^{***}p<0.001$ by unpaired t test. Data are presented as mean ± SEM

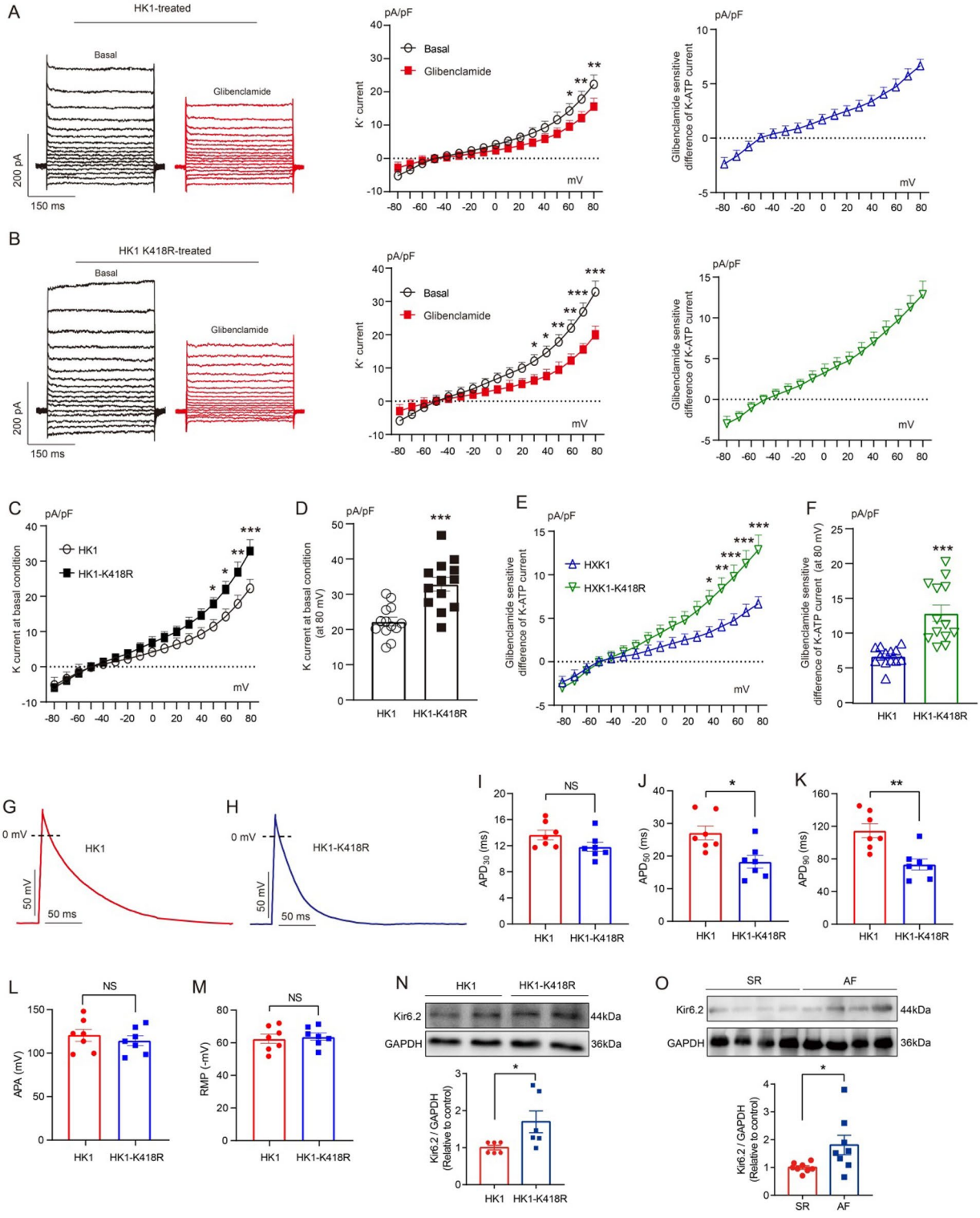

Fig. 5 (See legend on next page.)

(See figure on previous page.)

Fig. 5 HK1-K418R increased ATP-sensitive potassium channel current ($I_{K,ATP}$), reduced action potential duration (APD), and increased Kir6.2. (**A** and **B**) ATP-sensitive potassium current ($I_{K,ATP}$) was significantly inhibited by glibenclamide in HL-1 atrial myocytes ($n=13$) in both HK1 (22.26 ± 1.26 vs. 15.59 ± 1.14 pA/pF) and HK1-K418R (32.84 ± 1.95 vs. 19.98 ± 1.34 pA/pF) group. The left panel shows representative traces of whole-cell K^+ currents. The mid panel shows the comparison of K^+ currents with or without glibenclamide. The right panel shows the difference of the currents induced by glibenclamide ($I_{K,ATP}=I_{Basal}-I_{Glibenclamide}$). (**C** and **D**) Comparisons of currents at basic levels ($n=13$) between HK1 and HK1-K418R. The currents in HK1-K418R were significantly higher than that in HK from 50 to 80 mV. HK1-K418R increased whole-cell K + current from 22.26 ± 1.26 pA/pF to 32.84 ± 1.95 pA/pF. (**E** and **F**) Comparisons of glibenclamide-sensitive currents ($I_{K,ATP}$, $n=13$). The currents in HK1-K418R were significantly higher than that in HK from 40 to 80 mV. HK1-K418R increased $I_{K,ATP}$ current from 6.67 ± 0.37 to 12.89 ± 1.19 pA/pF. (**G** and **H**) HK1-K418R resulted in shortening of APD. (**I**, **L**, and **M**) HK1-K418R did not affect APD_{30}, APA, and RMP. (**J** and **K**) Compared to HK1, APD_{50} decreased from 27.11 ± 2.09 to 18.26 ± 1.93 ms ($n=7$) and APD_{90} decreased from 114.64 ± 8.67 to 73.21 ± 6.91 ms ($n=7$). (**N**) HK1-K418R overexpression significantly increased the expression of Kir6.2 ($n=6$) compared with HK1 normal overexpression group in HL-1 cell. (**O**) The expression of Kir6.2 ($n=8$) in human atrial tissue with AF is significantly higher than that in SR atrial tissue. HK1, hexokinase-1; AF, atrial fibrillation; SR, sinus rhythm; GAPDH, glyceraldehyde-3-phosphate dehydrogenase; APA, action potential amplitude; RMP, resting membrane potential; NS, not significant. *$p<0.05$; **$p<0.01$; ***$p<0.001$ by unpaired t test. Data are presented as mean ± SEM

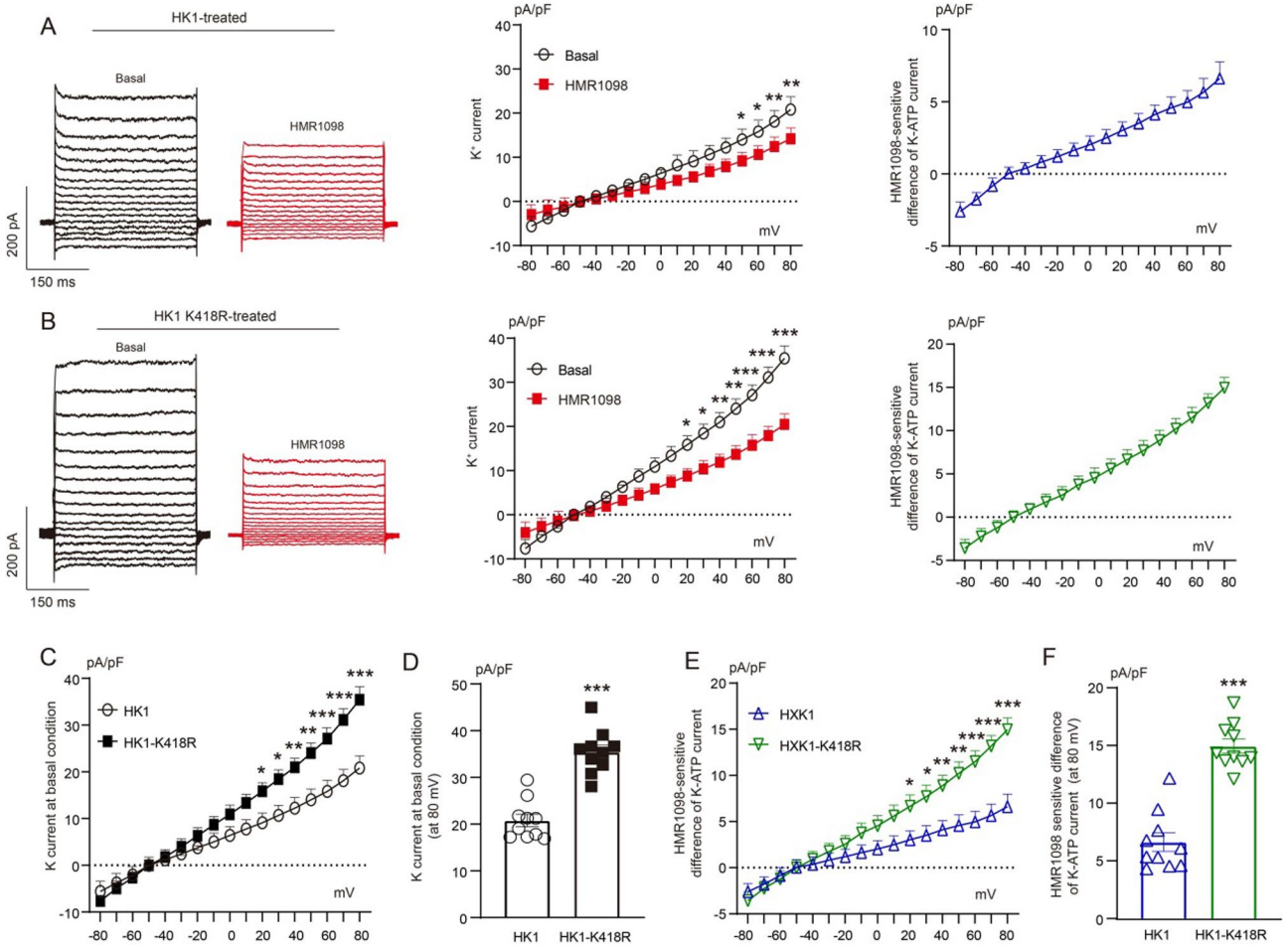

Fig. 6 HK1-K418R increased ATP-sensitive potassium channel current ($I_{K,ATP}$). (**A** and **B**) ATP-sensitive potassium current was significantly inhibited by HMR1098 in HL-1 atrial myocytes ($n=10$) in both HK1 and HK1-K418R. The left panel shows representative traces of whole-cell K^+ currents. The mid panel shows the comparison of K^+ currents with or without HMR1098. The right panel shows the difference of the currents induced by HMR1098 ($I_{K,ATP}=I_{Basal}-I_{HMR1098}$). (**C** and **D**) Comparisons of currents at basic levels ($n=10$) between HK1 and HK1-K418R. The currents in HK1-K418R were significantly higher than that in HK from 20 to 80 mV. HK1-K418R increased whole-cell K + current from 20.82 ± 1.32 pA/pF to 35.42 ± 1.46 pA/pF. (**E** and **F**) Comparisons of HMR1098-sensitive currents ($I_{K,ATP}$, $n=10$). The $I_{K,ATP}$ currents in HK1-K418R were significantly higher than that in HK from 20 to 80 mV. HK1-K418R increased $I_{K,ATP}$ currents from 6.62 ± 0.79 to 14.95 ± 0.62 pA/pF. *$p<0.05$; **$p<0.01$; ***$p<0.001$ by unpaired t test. Data are presented as mean ± SEM

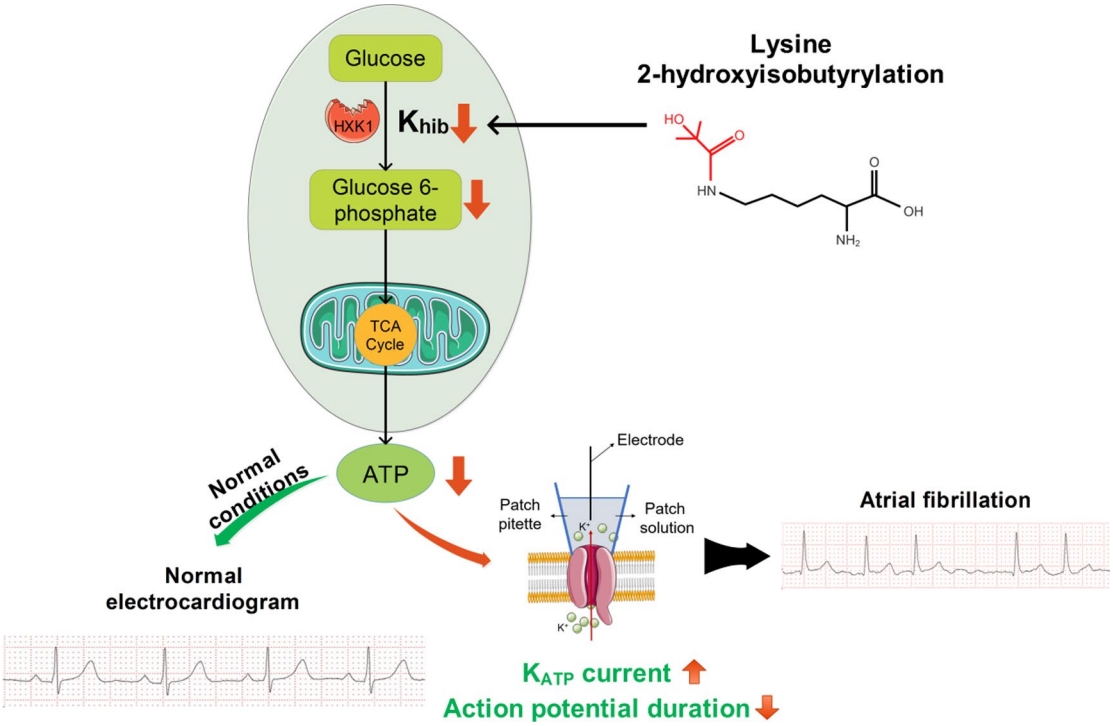

Fig. 7 Proposed mechanism of Lysine 2-hydroxyisobutyrylation modification of HXK1 leading to atrial fibrillation. Low lysine 2-hydroxyisobutyrylation level decreased catalytic activity of HXK1 and production of glucose-6-phosphate and ATP. These metabolic changes resulted in the increasing of ATP-sensitive potassium channel ($I_{K,\ ATP}$) currents and decreased action potential duration, triggering the onset of atrial fibrillation. HXK1, hexokinase 1; ATP, adenosine 5′-triphosphate

HXK1 activity and ATP generation that may trigger the development of AF.

Ca^{2+} handling [43] and mitochondrial energetics [45] play central roles in the initiation and maintenance of arrhythmic activity. Reduction of ATP from mitochondria causes subsequent Ca^{2+} overload and this may cause arrhythmia [45]. The present study revealed the relationship between arrhythmia and ATP from mitochondria and for the first time demonstrated the biological significance of K_{hib} in AF.

Energy metabolism of AF

AF is an energy challenge and is closely intertwined with metabolic abnormalities including fatty acid metabolism, glucose metabolism, and mitochondrial function. AF also triggers a metabolic switch from preferential fatty acid utilization to glucose metabolism to increase the efficiency of ATP produced in relation to oxygen consumed [46]. The energy substrate alternate can be as a potential therapeutic intervention [47]. The atrium has specific metabolic features (anatomy, cell constitutes, genetic phenotype, and metabolism), which are different to ventricle. Altered energy metabolism (substrate oxidation rates and mitochondrial dysfunctions) is closely related to atrial arrhythmogenesis [47].

Different risk factors for AF, including hypertension, aging, and diabetes, show metabolic abnormalities and exhibit different metabolic characteristics [46]. As to the clinical characteristics, the left atrial size is a significant factor related to AF, as demonstrated in many other studies [26, 27]. It is also reported that elevated levels of tricarboxylic acid cycle-related metabolites (succinate, malate, citrate, d/l-2-hydroxyglutarate, and aconitate) are associated with a higher risk of AF [48]. Impaired mitochondrial Ca^{2+} uniporter complex activity and mitochondrial Ca^{2+} homeostasis from the early stage of metabolic cardiomyopathy lead to AF [49]. Various pathophysiological mechanisms (HMGB1, heat shock proteins and S100 alarmins [50], and lncRNA TCONS_00016478 [51]) are also involved in AF progression.

Our study demonstrated the mechanism of AF from the perspective of K_{hib} PTM and we found 10 K_{hib} sites including in energy metabolism-related signaling transduction pathways (HXK1, TPIS, PGM1, and ODPX in glycolysis; MDHC and IDH3A in tricarboxylic acid cycle; NDUS2, ETFB, ADT3, and ATPB in oxidative respiratory chain). Further, we focused our study on the biological role of HXK1 K_{hib}, which is the key rate-limiting enzyme in glycolysis. Our study therefore provides new insights into the mechanism of AF from the view of protein PTM regarding energy metabolism.

HXK1 K418$_{hib}$ increased Kir6.2 and $I_{K,\ ATP}$ but decreased APD that likely triggers AF

It has been known that K_{ATP} channels have diverse physiological and pathophysiological functions in various cardiovascular components (atria, ventricles, endothelium, smooth muscle, specialized conduction system, and mitochondria) [37]. The molecular compositions of K_{ATP} channel in atrium are Kir6.2, SUR1, and SUR2A [37]. The activity of the K_{ATP} channel is inhibited by ATP [52] with binding to the Kir6.2 subunit [37] and provides a unique link between cellular energetics and electrical excitability [53]. K_{ATP} channel opening is also mediated by ATP/ADP (adenosine diphosphate) ratio, level of the channel microenvironment, and glycolysis, and it is directly associated with glycolytic enzymes [37]. In the cardiovascular system, the ATP sensitivity is higher in the atrium and ventricle than that in other tissues [37]. In general, K_{ATP} channel activation should probably be considered as pro-arrhythmic [37, 54], but an argument is that K_{ATP} channel activation may be anti-arrhythmic [37].

The exact shape and duration of AP are regulated by subtle interplay of different ion channels. The initial fast depolarization is obtained by opening of voltage-dependent Na^+ channel and the repolarization is characterized by inward Ca^{2+} and outward K^+ currents. The APD is mainly determined by the balance of Ca^{2+} and K^+ currents. Increase of K^+ current is related to shortening APD [55]. K_{ATP} current is activated during the entire period of the AP and it is one of important outward K^+ current during repolarization of atrium; therefore the change of K_{ATP} current affects APD, i.e., increased K_{ATP} current shortens APD. Consequently, decreased APD induces triangulation, which increases the vulnerable window and therefore is a pro-arrhythmic biomarker. APD shortening caused by ion channel dysfunction results in short effective refractory period, and effective refractory period shortening promotes re-entry, which is a mechanism underlying arrhythmogenesis [56].

In this study, by linking the HXK1 K418$_{hib}$ and the altered K_{ATP} current, we for the first time report that HXK1 K418$_{hib}$ reduced HXK1 activity, resulting in lower production of glucose-6-phosphate and ATP that significantly increased Kir6.2 and $I_{K,\ ATP}$, and decreased APD_{50} and APD_{90}. These changes finally trigger the onset of AF. The activation of K_{ATP} current and shortening of APD are in consistent with other studies [57–59].

Limitations of study

K_{ATP} channels have certain connections with Ca^{2+} channels [53]. Functional studies to elucidate the role HXK1 K418$_{hib}$, Ca^{2+} channels, and K_{ATP} channels in cardiac cells are warranted.

There are a total of 10 regulated enzymes related to K_{hib} involved in glycolysis, TCA circle, and oxidative respiratory chain in this study. Apart from HXK1, the other K_{hib} sites should also be further studied.

In addition, this study is an in vitro investigation at the tissue and cellular level, the role of K_{hib} on the pathogenesis of AF in vivo should be further investigated.

Conclusions

In summary, through quantitative K_{hib} proteomics and functional metabolic analysis, this study discovered ten energy metabolism-related K_{hib} modification sites (HXK1, TPIS, PGM1, and ODPX in glycolysis; MDHC and IDH3A in TCA circle; NDUS2, ETFB, ADT3, and ATPB in oxidative respiratory chain) between SR and AF. In particular, HXK1 K418$_{hib}$ reduced HXK1 activity, resulting in lower production of glucose-6-phosphate and ATP that increases Kir6.2 and $I_{K,\ ATP}$ but decreases APD. These changes likely play an important role in the triggering of the onset of AF.

Abbreviations

ADP	Adenosine diphosphate
ATP	Adenosine 5′-triphosphate
AF	Atrial fibrillation
BMI	Body massive index
GAPDH	Glyceraldehyde-3-phosphate dehydrogenase
HDACs	Histone deacetylases
HXK1	Hexokinase-1
GO	Gene Ontology
LAD	Left atrial diameter
LVDD	Left ventricular diastolic disorder
LVEF	Left ventricular ejection fraction
KEGG	Kyoto Encyclopedia of Genes and Genomes
K_{hib}	Lysine 2-hydroxyisobutyrylation
MS	Mass spectrometry
MWCO	Molecular weight cut-off
NADH	Nicotinamide adenine dinucleotide
PPAR	Peroxisome proliferator-activated receptor
SR	Sinus rhythm
TCA	Tricarboxylic acid cycle
TMT	Tandem mass tag

Supplementary Information

The online version contains supplementary material available at https://doi.org/10.1186/s12964-025-02108-z.

Supplementary Material 1: Figure S1. Functional annotation and enrichment analysis of GO categories and KEGG using differentially-2-hydroxyisobutyrylated proteins. Figure S2. Enrichment-based hierarchical cluster analysis based on different fold change. Table S1. Multivariate logistic regression analysis: independent risk factors for AF in patients with heart valvular disease.

Acknowledgements

We thank all the nurses for the assistance of collecting samples, Department of Cardiovascular Surgery, TEDA International Cardiovascular Hospital, Tianjin, China.

Author contributions

G.W.H. conceived the whole study. H.T.H. and X.C.W. performed the experiments. H.T.H. and G.W.H. wrote the manuscript. H.T.H, X.C.W, J.W. collected the samples. H.T.H, H.X.C, J.W, and Q.Y. prepared materials for experiments. H.T.H., Q.Y., G.W.H. discussed the study protocols, the process of

the experiments, and the manuscript. G.W.H. had overall responsibility for the whole study. All authors approved the final manuscript version.

Funding
This work was supported by grants from the National Natural Science Foundation of China [82170353 & 82370350 & 81870288]; Tianjin Science and Technology Commission [22ZYQYSY00020 & 21JCYBJC01120]; the Non-profit Central Research Institute Fund of Chinese Academy of Medical Sciences [2020-PT310-007 & 2019XK310001], China Post-doctoral Science Foundation [2021M692374], and Special Fund for High Quality Development Project.

Data availability
The mass spectrometry proteomics data have been deposited in the ProteomeXchange Consortium via the PRIDE partner repository with the data set identifier PXD032154.

Declarations

Competing interests
The authors declare no competing interests.

Received: 13 August 2024 / Accepted: 14 February 2025
Published online: 03 March 2025

References

1. Nattel S, Atrial Fibrillation and Body Composition. Is it fat or lean that ultimately determines the risk?? J Am Coll Cardiol. 2017;69:2498–501.
2. Lazarte J, Laksman ZW, Wang J, Robinson JF, Dron JS, Leach E, Liew J, McIntyre AD, Skanes AC, Gula LJ, et al. Enrichment of loss-of-function and copy number variants in ventricular cardiomyopathy genes in 'lone' atrial fibrillation. Europace. 2021;23:844–50.
3. Kirchhof P, Benussi S, Kotecha D, Ahlsson A, Atar D, Casadei B, Castella M, Diener HC, Heidbuchel H, Hendriks J, et al. 2016 ESC guidelines for the management of atrial fibrillation developed in collaboration with EACTS. Eur Heart J. 2016;37:2893–962.
4. Thorolfsdottir RB, Sveinbjornsson G, Sulem P, Helgadottir A, Gretarsdottir S, Benonisdottir S, Magnusdottir A, Davidsson OB, Rajamani S, Roden DM, et al. A missense variant in PLEC increases risk of atrial fibrillation. J Am Coll Cardiol. 2017;70:2157–68.
5. Zhang D, Wu CT, Qi X, Meijering RA, Hoogstra-Berends F, Tadevosyan A, Cubukcuoglu Deniz G, Durdu S, Akar AR, Sibon OC, et al. Activation of histone deacetylase-6 induces contractile dysfunction through derailment of α-tubulin proteostasis in experimental and human atrial fibrillation. Circulation. 2014;129:346–58.
6. Olson TM, Michels VV, Ballew JD, Reyna SP, Karst ML, Herron KJ, Horton SC, Rodeheffer RJ. Anderson JL sodium channel mutations and susceptibility to heart failure and atrial fibrillation. JAMA. 2005;293:447–54.
7. Dobrev D, Friedrich A, Voigt N, Jost N, Wettwer E, Christ T, Knaut M, Ravens U. The G protein-gated potassium current I(K,ACh) is constitutively active in patients with chronic atrial fibrillation. Circulation. 2005;112:3697–706.
8. Jiang YY, Hou HT, Yang Q, Liu XC, He GW. Chloride channels are involved in the development of atrial Fibrillation - A transcriptomic and proteomic study. Sci Rep. 2017;7:10215.
9. Li XY, Hou HT, Chen HX, Liu XC, Wang J, Yang Q. He GW preoperative plasma biomarkers associated with atrial fibrillation after coronary artery bypass surgery. J Thorac Cardiovasc Surg. 2021;162:851– 63.e3.
10. Skalidis EI, Hamilos MI, Karalis IK, Chlouverakis G, Kochiadakis GE. Vardas PE isolated atrial microvascular dysfunction in patients with lone recurrent atrial fibrillation. J Am Coll Cardiol. 2008;51:2053–7.
11. Chen HX, Li MY, Jiang YY, Hou HT, Wang J, Liu XC, Yang Q, He GW. Role of the PPAR pathway in atrial fibrillation associated with heart valve disease: transcriptomics and proteomics in human atrial tissue. Signal Transduct Target Ther. 2020;5:4.
12. Dai L, Peng C, Montellier E, Lu Z, Chen Y, Ishii H, Debernardi A, Buchou T, Rousseaux S, Jin F, et al. Lysine 2-hydroxyisobutyrylation is a widely distributed active histone mark. Nat Chem Biol. 2014;10:365–70.
13. Xie Z, Zhang D, Chung D, Tang Z, Huang H, Dai L, Qi S, Li J, Colak G, Chen Y, et al. Metabolic regulation of gene expression by histone lysine β-Hydroxybutyrylation. Mol Cell. 2016;62:194–206.
14. Tan M, Luo H, Lee S, Jin F, Yang JS, Montellier E, Buchou T, Cheng Z, Rousseaux S, Rajagopal N, et al. Identification of 67 histone marks and histone lysine crotonylation as a new type of histone modification. Cell. 2011;146:1016–28.
15. Zhang Z, Tan M, Xie Z, Dai L, Chen Y, Zhao Y. Identification of lysine succinylation as a new post-translational modification. Nat Chem Biol. 2011;7:58–63.
16. Tan M, Peng C, Anderson KA, Chhoy P, Xie Z, Dai L, Park J, Chen Y, Huang H, Zhang Y, et al. Lysine glutarylation is a protein posttranslational modification regulated by SIRT5. Cell Metab. 2014;19:605–17.
17. Goudarzi A, Zhang D, Huang H, Barral S, Kwon OK, Qi S, Tang Z, Buchou T, Vitte AL, He T, et al. Dynamic competing histone H4 K5K8 acetylation and butyrylation are hallmarks of highly active gene promoters. Mol Cell. 2016;62:169–80.
18. Lin YY, Kiihl S, Suhail Y, Liu SY, Chou YH, Kuang Z, Lu JY, Khor CN, Lin CL, Bader JS, et al. Functional dissection of lysine deacetylases reveals that HDAC1 and p300 regulate AMPK. Nature. 2012;482:251–5.
19. Sabari BR, Zhang D, Allis CD, Zhao Y. Metabolic regulation of gene expression through histone acylations. Nat Rev Mol Cell Biol. 2017;18:90–101.
20. Huang H, Tang S, Ji M, Tang Z, Shimada M, Liu X, Qi S, Locasale JW, Roeder RG, Zhao Y et al. p300-Mediated lysine 2-Hydroxyisobutyrylation regulates Glycolysis. Mol Cell. 2018;70:663– 78.e6.
21. Zhang N, Zhang L, Li L, Geng J, Zhao L, Ren Y, Dong Z, Chen F. Global profiling of 2-hydroxyisobutyrylome in common wheat. Genomics Proteom Bioinf. 2022;20:688–701.
22. Huang J, Luo Z, Ying W, Cao Q, Huang H, Dong J, Wu Q, Zhao Y, Qian X, Dai J. 2-Hydroxyisobutyrylation on histone H4K8 is regulated by glucose homeostasis in Saccharomyces cerevisiae. Proc Natl Acad Sci U S A. 2017;114:8782–7.
23. Chen X, Xu Q, Duan Y, Liu H, Chen X, Huang J, Luo C, Zhou DX. Zheng L ustilaginoidea virens modulates lysine 2-hydroxyisobutyrylation in rice flowers during infection. J Integr Plant Biol. 2021;63:1801–14.
24. Bai F, Tu T, Qin F, Ma Y, Liu N, Liu Y, Liao X, Zhou S, Liu Q. Quantitative proteomics of changes in succinylated proteins expression profiling in left appendages tissue from valvular heart disease patients with atrial fibrillation. Clin Chim Acta. 2019;495:345–54.
25. Rossi A, Rigotto G, Valente G, Giorgio V, Basso E, Filadi R, Pizzo P. Defective mitochondrial pyruvate flux affects cell bioenergetics in Alzheimer's Disease-Related models. Cell Rep. 2020;30:2332–48. e10.
26. Vaziri SM, Larson MG, Benjamin EJ, Levy D. Echocardiographic predictors of nonrheumatic atrial fibrillation. Framingham Heart Study Circulation. 1994;89:724–30.
27. Bisbal F, Alarcón F, Ferrero-de-Loma-Osorio A, González-Ferrer JJ, Alonso C, Pachón M, Tizón H, Cabanas-Grandío P, Sanchez M, Benito E, et al. Left atrial geometry and outcome of atrial fibrillation ablation: results from the multicentre LAGO-AF study. Eur Heart J Cardiovasc Imaging. 2018;19:1002–9.
28. Claycomb WC, Lanson NA Jr., Stallworth BS, Egeland DB, Delcarpio JB, Bahinski A, Izzo NJ Jr. HL-1 cells: a cardiac muscle cell line that contracts and retains phenotypic characteristics of the adult cardiomyocyte. Proc. Natl. Acad. Sci. U. S. A. 1998;95:2979-84.
29. Yang Z, Shen W, Rottman JN, Wikswo JP. Murray KT rapid stimulation causes electrical remodeling in cultured atrial myocytes. J Mol Cell Cardiol. 2005;38:299–308.
30. Yang T, Wathen MS, Felipe A, Tamkun MM, Snyders DJ. Roden DM K + currents and K + channel mRNA in cultured atrial cardiac myocytes (AT-1 cells). Circ Res. 1994;75:870–8.
31. Yue L, Feng J, Gaspo R, Li GR, Wang Z, Nattel S. Ionic remodeling underlying action potential changes in a canine model of atrial fibrillation. Circ Res. 1997;81:512–25.
32. Yagi T, Pu J, Chandra P, Hara M, Danilo P Jr., Rosen MR. Boyden PA density and function of inward currents in right atrial cells from chronically fibrillating canine atria. Cardiovasc Res. 2002;54:405–15.
33. Bosch RF, Zeng X, Grammer JB, Popovic K, Mewis C. Kühlkamp V ionic mechanisms of electrical remodeling in human atrial fibrillation. Cardiovasc Res. 1999;44:121–31.
34. Maharani N, Ting YK, Cheng J, Hasegawa A, Kurata Y, Li P, Nakayama Y, Ninomiya H, Ikeda N, Morikawa K, et al. Molecular mechanisms underlying Urate-Induced enhancement of Kv1.5 channel expression in HL-1 atrial myocytes. Circ J. 2015;79:2659–68.
35. Wang XC, Jia QZ, Yu YL, Wang HD, Guo HC, Ma XD, Liu CT, Chen XY, Miao QF, Guan BC, et al. Inhibition of the I(Na/K) and the activation of peak I(Na) contribute to the arrhythmogenic effects of aconitine and Mesaconitine in guinea pigs. Acta Pharmacol Sin. 2021;42:218–29.

36. Wang XC, Sun WT, Yu CM, Pun SH, Underwood MJ, He GW. Yang Q ER stress mediates homocysteine-induced endothelial dysfunction: modulation of IKCa and SKCa channels. Atherosclerosis. 2015;242:191–8.
37. Foster MN. Coetzee WA KATP channels in the cardiovascular system. Physiol Rev. 2016;96:177–252.
38. Chen XF, Chen X, Tang X. Short-chain fatty acid, acylation and cardiovascular diseases. Clin Sci (Lond). 2020;134:657–76.
39. Travers JG, Wennersten SA, Peña B, Bagchi RA, Smith HE, Hirsch RA, Vanderlinden LA, Lin YH, Dobrinskikh E, Demos-Davies KM, et al. HDAC Inhibition reverses preexisting diastolic dysfunction and blocks Covert extracellular matrix remodeling. Circulation. 2021;143:1874–90.
40. Zhang D, Hu X, Henning RH. Brundel BJ keeping up the balance: role of HDACs in cardiac proteostasis and therapeutic implications for atrial fibrillation. Cardiovasc Res. 2016;109:519–26.
41. Chang CJ, Li SJ, Chen YC, Huang SY, Chen SA, Chen YJ. Histone deacetylase Inhibition attenuates atrial arrhythmogenesis in sterile pericarditis. Transl Res. 2018;200:54–64.
42. Seki M, LaCanna R, Powers JC, Vrakas C, Liu F, Berretta R, Chacko G, Holten J, Jadiya P, Wang T, et al. Class I histone deacetylase Inhibition for the treatment of sustained atrial fibrillation. J Pharmacol Exp Ther. 2016;358:441–9.
43. Harada M, Tadevosyan A, Qi X, Xiao J, Liu T, Voigt N, Karck M, Kamler M, Kodama I, Murohara T, et al. Atrial fibrillation activates AMP-Dependent protein kinase and its regulation of cellular calcium handling: potential role in metabolic adaptation and prevention of progression. J Am Coll Cardiol. 2015;66:47–58.
44. Chakraborty P, Nattel S, Nanthakumar K. Linking cellular energy state to atrial fibrillation pathogenesis: potential role of adenosine monophosphate-activated protein kinase. Heart Rhythm. 2020;17:1398–404.
45. Mason FE, Pronto JRD, Alhussini K, Maack C, Voigt N. Cellular and mitochondrial mechanisms of atrial fibrillation. Basic Res Cardiol. 2020;115:72.
46. Qin X, Zhang Y, Zheng Q. Metabolic inflexibility as a pathogenic basis for atrial fibrillation. Int J Mol Sci. 2022;23.
47. Lkhagva B, Lee TW, Lin YK, Chen YC, Chung CC, Higa S, Chen YJ. Disturbed cardiac metabolism triggers atrial arrhythmogenesis in diabetes mellitus: energy substrate alternate as a potential therapeutic intervention. Cells. 2022;11.
48. Bulló M, Papandreou C, García-Gavilán J, Ruiz-Canela M, Li J, Guasch-Ferré M, Toledo E, Clish C, Corella D, Estruch R, et al. Tricarboxylic acid cycle related-metabolites and risk of atrial fibrillation and heart failure. Metabolism. 2021;125:154915.
49. Fossier L, Panel M, Butruille L, Colombani S, Azria L, Woitrain E, Decoin R, Torrente AG, Thireau J, Lacampagne A, et al. Enhanced mitochondrial calcium uptake suppresses atrial fibrillation associated with metabolic syndrome. J Am Coll Cardiol. 2022;80:2205–19.
50. Imbalzano E, Murdaca G, Orlando L, Gigliotti-De Fazio M, Terranova D, Tonacci A, Gangemi S. Alarmins as a possible target of future therapies for atrial fibrillation. Int J Mol Sci. 2022;23.
51. Jiang W, Xu M, Qin M, Zhang D, Wu S, Liu X, Zhang Y. Study on the role and mechanism of LncRNA in the remodeling of atrial energy metabolism in rabbits with atrial fibrillation based on nano sensor technology. Bioengineered. 2022;13:863–75.
52. Aguilar-Bryan L, Bryan J. Molecular biology of adenosine triphosphate-sensitive potassium channels. Endocr Rev. 1999;20:101–35.
53. Nichols. CG KATP channels as molecular sensors of cellular metabolism. Nature. 2006;440:470–6.
54. Flagg TP, Enkvetchakul D, Koster JC, Nichols CG. Muscle KATP channels: recent insights to energy sensing and myoprotection. Physiol Rev. 2010;90:799–829.
55. Grunnet M. Repolarization of the cardiac action potential. Does an increase in repolarization capacity constitute a new anti-arrhythmic principle? Acta Physiol (Oxf). 2010;198(Suppl 676):1–48.
56. Hanna MS, Coromilas J, Josephson ME, Wit AL. Peters NS mechanisms of resetting reentrant circuits in canine ventricular tachycardia. Circulation. 2001;103:1148–56.
57. Chan CS, Lin YK, Kao YH, Chen YC, Chen SA, Chen YJ. Hydrogen sulphide increases pulmonary veins and atrial arrhythmogenesis with activation of protein kinase C. J Cell Mol Med. 2018;22:3503–13.
58. Lee CC, Chang SN, Tehrani B, Liu SS, Chan CY, Hsu WT, Huang TY, Huang PS, Hwang JJ, Chen JJ, et al. Use of Nicorandil is associated with increased risk of incident atrial fibrillation. Aging (Albany N Y). 2022;14:6975–92.
59. Suffee N, Baptista E, Piquereau J, Ponnaiah M, Doisne N, Ichou F, Lhomme M, Pichard C, Galand V, Mougenot N, et al. Impacts of a high-fat diet on the metabolic profile and the phenotype of atrial myocardium in mice. Cardiovasc Res. 2022;118:3126–39.

Publisher's note